Influence of dc pulsed atmospheric pressure plasma jet processing conditions on polymer activation

D. P. Dowling[1], F. T. O'Neill[1], S. J. Langlais[1], and V. J. Law[2]

[1]School of Mechanical and Materials Engineering, University College Dublin, Belfield, Dublin 4, Ireland

[2]Dublin City University, National Center of Plasma Science and Technology, Collins Avenue, Glasnevin, Dublin 9, Dublin, Ireland

denis.dowling@ucd.ie

Abstract

Plasma treatments are widely used to activate polymer surfaces prior to adhesive bonding. This study investigates the influence of plasma treatment conditions on the surface activation of a range of polymers using the PlasmaTreat (Open Air) system. In this study the effect of dc pulse plasma cycle time, compressed air flow rate and the plasma jet nozzle to substrate distance on the activation of polypropylene, polystyrene and polycarbonate were investigated. The level of polymer surface activation was evaluated based on the change in water contact angle after plasma treatment. The polymer surface properties were also monitored using AFM and XPS measurements. The heating effect of the plasma was monitored using both infrared thermographic camera and thermocouple measurements. Plasma diagnostics measurements were obtained using the photo-diode and optical emission spectroscopy techniques. From this study it was concluded that for the PlasmaTreat system the level of plasma activation was closely correlated with the dc pulsed plasma cycle time, which is a measure of the plasma intensity. For example, the more intense plasma obtained with shorter cycle times gave higher levels of polymer activation. The optimized pulsed plasma cycle times were found to be specific for a given polymer type and related to their thermal properties. The pulsed cycle times were also found to correlate with both the substrate and plasma gas temperatures.

Keywords: Atmospheric plasma jet, water contact angle, plasma diagnostics and polypropylene

1 Introduction

Polymers generally have low surface energy [1] leading to problems such as poor wettability, dyeability and adhesion. A large range of techniques have been used to overcome this problem. These include the use of chemical treatments [2], flame [3], corona [4] as well as both low pressure and atmospheric pressure plasmas [5, 6]. A particular advantage of plasma treatments for activating polymers is the uniformity of the treatment [7]. The depth of modification with plasma treatments is generally less than 10 nm [8]. One of its effects is to enhance crosslinking and as a result weak boundary layers can be removed, hence strengthening the adhesive bond [9]. Chain scissioning of the long polymer molecules may also occur, thus generating chemical sites which are available for bonding with an adhesive. For example the incorporation of functional groups containing oxygen and nitrogen into the surface has been demonstrated after plasma activation [10]. It has been shown that even if only a few chemical sites are created there will be a large increase in adhesive strength [11]. Removal of surface contaminants is also an important contribution of plasma treatment to polymer adhesion [12].

A key issue is to maximise the level of plasma activation (generally associated with the greatest reduction in water contact angle), while preventing thermal damage to the polymer substrate. This paper is focussed on using plasma diagnostic techniques (optical emission spectroscopy and photo diode light measurements) as a method of monitoring the plasma activation process. The treatment studies were carried out using a commercial atmospheric pressure air plasma system called PlasmaTreat^{TM}. Amongst the

plasma activation studies reported to-date with this source are those that aim to enhance the surface energy of polyethylene prior to adhesive bonding [13], adhesion improvement [6] and textile polymer treatments [14]. This source has also been used in the deposition of plasma polymerized coatings for gas barrier applications [15] and corrosion protection [16, 17]. These papers have mainly focused on the process outcome as a function of anode-nozzle speeds relative to the treated surface. To prevent thermal surface damage, the anode-nozzle-to-surface gap is reported to be in the range of 50 to 80 mm for static treatment, however this gap distance can be reduced to 10-20 mm, when the discharge was moved rapidly (10 to 80 $m.min^{-1}$) over the surface. To date there have been very few reports on the use of plasma diagnostic techniques to examine the PlasmaTreat system. An example is reference [13] which establishes that the NO_2* continuum within the flowing afterglow played an important role in the treatment of polyethylene surface adhesion improvement. In this study plasma diagnostic measurements are correlated with the heating effect of the PlasmaTreat plasma jet and the level of activation of polymer surfaces for the first time.

Polymers often have differing thermal properties therefore this study was carried out using three polymers, polypropylene (PP), polystyrene (PS) and polycarbonate (PC). These polymers have typical glass transition temperatures (Tg) of approximately 13, 90 and 150°C, respectively [18, 19]. This work investigates the modification of the water contact angle of these polymers, as a function of the atmospheric plasma jet discharge parameters: air volume flow, anode-nozzle-to-surface gap distance and plasma cycle time (PCT). The latter parameter is a measure of the plasma intensity and is described in the Experimental section. These parameters were correlated with optical emission spectroscopy and the polychromic light intensity measurements of the discharge. These measurement techniques were chosen as the discharge has a small electric field ($mV.cm^{-1}$) outside the arc region and is therefore difficult to analyze without distorting this discharge. As the treated materials are thermoplastic polymer resins, the treatment temperature is of particular importance [3, 4, 20 and 21]. Therefore the system temperature was also measured as a function of afterglow axial position.

Experimental Details

Equipment and materials

The plasma activation studies were carried out using the OpenAir system manufactured by PlasmaTreat GmbH (Steinhagen, Germany). A number of authors have previously described the operation of this atmospheric pressure plasma jet (APPJ) source [13-17]. A schematic diagram of the system is given in Figure 1, this illustrates how the blown arc is formed inside the arc cavity and ionized gas is expelled through the anode-nozzle [22 and 23]. The photograph of the anode-nozzle region which is also included in this figure, illustrates the blown arc protruding from the nozzle as an intense bright-white region, surrounded by a corona-like discharge. As the gas is blown through this region a flowing afterglow is formed that takes on a yellow-orange feathered appearance. This system is also equipped with a liquid precursor delivery system but this is not used in this study.

The working gas is dry compressed air, with an inlet pressure between 100,000 to 300,000 Pascal. Using a PFW10 anode-nozzle the volume flow rate ranges were evaluated between 37.5 to 76.6 l/s. The plasma applicator is mounted onto a XYZ gantry which allows the discharge plume to target a 2-dimensional or 3-dimensional process part at parallel speeds of 0 to 30 $m.min^{-1}$. The polymer treatment time was thus less than 0.1 seconds for a given point on the polymer surface (mounted on a ceramic plate). In this study the substrate to jet anode-nozzle distance (gap distance) was varied between 10 and 24 mm. Some studies were carried out at a fixed gap distance, for these experiments the polymer to nozzle orifice distance was maintained at 16 mm.

The APP jet is driven by a uni-polar square-wave pulse-width modulation (PWM) transistor amplifier circuit. This circuit provides an immediate amount of electrical power between fully on and fully off [24] at a drive switching frequency between 17 to 25 kHz. The PWM waveform is amplified through a step-up transformer to provide a peak dc pulse voltage of 2 to 5 kV. Varying the square-wave pulse on-time (t_{on}) and the number of pulses per unit time creates a Root Mean Square (RMS) direct current (dc) level that controls the average dc power that is delivered to the discharge reactor. This circuit topology is a very efficient means of controlling electrical power because the power transistors dissipate comparatively little power when they are switched on and off. When the transistor is in cutoff, its power dissipation is zero because no current passes through it. For the purpose of clarity the manufacturer uses the term Plasma Cycle Time (PCT) in controlling the RMS pulse level. The PCT level therefore determines the effective duty cycle. This is broadly similar to the operation of low frequency (e.g. 300 kHz) pulse plasma processing, where a repetitive series of pulses is turned on and off with varying off time to produce a pulse chain that can be mathematically characterized by the duty cycle $d = t_{on}/t_p$. Where t_p is the period of the PWM drive frequency ($t_p = 1/f$) [25, 26]. As the PWM power supply is designed to provide a time average dc level via a sequence of dc pulses, it therefore becomes necessary to monitor the varying pulse sequence as a function of PWM drive frequency.

Polymer surface characterization

The plasma activation studies were carried out on polypropylene, polystyrene and polycarbonate substrates obtained from AB Suppliers Ltd (UK). These polymers had thicknesses of 50, 500 and 100 μm, respectively. Contact angle measurements were obtained both immediately after plasma treatment and also at varying times after treatment, in order to measure hydrophobic recovery [27]. Coating contact angles were measured using de-ionized water at room temperature using a video capture apparatus OCA 20 from Dataphysics Instruments. Surface morphology examination was also carried out using a CP-II (Veeco) Atomic Force Microscope (AFM) operating in non contact mode. The average (*Ra*) and root mean square (*Rq*) surface roughness reported was obtained by taking the mean of five measurements on different areas (5 x 5 μm of each sample. X-ray photoelectron

spectroscopy (XPS) was performed using a Kratos Analytical Axis Ultra photoelectron spectrometer. This instrument has a spherical mirror analyzer with an integrated automatic charge neutralizer and a magnetic lens. A monochromated (Al Kα) x-ray source was used to record spectra at normal emission. The area analysed was 700 x 300 μm with a take-off-angle of 90°. The elemental composition is presented as the average of three analyses. Each position was analysed in the survey mode (Pass Energy 160 eV) to determine the elements present at the surface and their relative concentrations. CasaXPS (Casa Software Ltd) data processing software was used to calculate the area under peaks representative of elements detected, which were then normalized to take into account relative sensitivity to provide relative concentrations.

Thermal measurements

Infra red thermal imaging of both the anode-nozzle and surface were obtained using an InfraTec VarioCAM high resolution infrared thermographic camera. The measurement procedure is similar to that reported previously [28 and 29], where the reactor cylinder wall was investigated. To provide an alternative method of temperature measurement of the discharge treated surface, thermocouple measurements (K-type) where performed on a ceramic surface at an anode-nozzle to substrate distance of 16 mm. An alumina ceramic surface ((W)21cm, (L)27cm and (H)0.4cm) was chosen as the comparative target as it has high specific heat capacity (850 J/g K) and thus avoids potential thermal degradation issues that can occur for polymer surfaces after extended exposure to the jet.

Plasma diagnostic measurements

These were obtained using both the photo-diode (PD) and optical emission spectroscopy (OES) techniques. The PD measurements were obtained using a Hamamatsu MPPC photo-diode, with a rise time of 10 ns and a spectral range between 320 to 900 nm. This system was used to measure the time varying polychromic emission intensity of the discharge. The discharge polychromic emission was collected via a fibre optic cable and collimating lens mounted in-line with (and focused on) the discharge flowing near-afterglow and along its axial axis in to the flowing far-afterglow. The analogue output of the spectrometer is connected via a National Instruments digitizer (-3 dB 100 MHz bandwidth), from where the signal is sent the computer where it is sampled and processed by a LabVIEW (National Instruments Corp.) software program.

The optical emission from the discharge was monitored using two Ocean Optics OES spectrometers. The HR4000 covers the 295–395 nm spectral region with a resolution of 0.12 nm full width at half maximum (FWHM), and a USB4000 UV/VIS spectrometer is used to cover the 200–850 nm region, with a resolution of 1.2 nm FWHM. The spectra where captured using an average of 4 traces and an integration time of 100 to 400 ns. A qualitative overview of the discharge chemistry is obtained from the 200–850 nm data by analyzing the observed line and band emission intensities resulting from different excitation and ionization processes in the discharge. The spectral lines where assigned according to Pearse and Greydon [30]. The rotational temperature of the nitrogen molecules in the discharge were determined from the high resolution OES data. This method is based on fitting a simulated spectrum to the measurement points and is described in detailed elsewhere [31]. The N_2 $v = 0 \rightarrow 2$ rotational band ($C^3\Pi^+_u - B^3\Pi^+_g$) at λ = 380 nm second positive system of molecular nitrogen is used as the small quantum numbers of the states means that their population distribution is likely to be closer to equilibrium.

Results and Discussion

Real-time plasma analysis

OES measurements

The blown arc and flowing afterglow region was temporally and spatially characterized using OES polychromic light emission studies. The low resolution OES survey as a function of fixed axial position (0, 5, 10, 15 mm), within the discharge afterglow is shown in Figure 2. Note the 0 mm data is offset by +300 for clarity. This figure reveals two contrasting emission regions. The region closes to the anode-nozzle contains NOγ bands (λ = 236-258 nm), the second positive system of molecular N_2 ($C^3\Pi^+u$-$B^3\Pi^+_g$) and at λ = 391 nm the $v = 0 \rightarrow 0$ band of the first positive nitrogen ions N_2^+ ($B^2\Sigma^+u$-$X^2\Sigma^+_g$) is observed. At longer wavelengths atomic H-Balmar-α line at λ = 656 nm, nitrogen and the O ($3p^5P$–$3s^5S$) at λ = 777 nm are also present. A feature of note here is that the atomic oxygen line has a similar intensity of the λ = 337 molecular N_2 line.

Moving away from the anode-nozzle along the discharge axis the optical emission undergoes an abrupt change in emission content at 5 mm, under the processing conditions used. Here, the excited NO_2* molecule (λ = 450-800 nm) continuum is formed with the second positive system of molecular N_2 and atomic oxygen are greatly reduced and the NOγ bands are still maintained. Continuing along the discharge axis-line to 10 mm the NO_2* continuum has decreased in intensity and the NOγ band are no longer present. At 15 mm, the NO_2* continuum intensity at 550 nm has decayed by a one half of that obtained at the 5 mm value. Further measurements (not shown here) indicate the continuum intensity (at 550 nm) has a discharge axial decay half-life value of $t_{1/2}$ ~ 15 mm. A further feature of note of these extended gap distance is that the second positive system of molecular N_2 at λ = 315 nm has an equally intensity to NO_2* continuum maximum.

These results provide a more detailed description of the discharge species as a function of discharge axial position than previously reported [13]. While this OES data provides information on the chemistry of the active species in the discharge, it is however limited in temperature information. In this work the temperature of the second positive system of molecular N_2 is determined using a high resolution OES survey. Typical optical emission spectra in the arc region (0-3 mm from the Anode-nozzle) was obtained for three PWM drive frequencies (19, 21 and 25 kHz) at a PCT = 100(%).

For the arc region, the rotational temperature of the nitrogen molecules were determined from the ($v = 0 \rightarrow 2$) emission bands of the second positive system of molecular nitrogen at λ = 380 nm. The method is based on fitting simulated spectra to the measurement points and is described in detail elsewhere [31]. The 380 nm line has been chosen since it has been found to be free from overlap with other spectral features and the small quantum number of the states means that their population distribution is likely to be closer to equilibrium. Using this procedure the rotational temperature is found to be in the range of 1709 ±100^{o}C at 25 kHz to 1761 ±100^{o}C at 19 kHz. When these nitrogen rotational temperatures for the PlasmaTreat system are compared with similar blown arc devices that use argon as the working gas, it is noted that this air based system operates in a temperature regime that is 5 -10 times lower than obtained with argon [23].

The OES measurements demonstrate that as the air is pushed through the arc region nitrous oxide, (NO) is formed, which then undergoes partial oxidation to the excited NO_2* state within the flowing afterglow. This process is represented by the NO-O chemiluminescent reaction (1) [13, 32, 33, and 34].

$$NO + O \rightarrow NO_2^* + h\nu \qquad (1)$$

Penetrante et al [33] has analyzed this reaction within oxygen rich atmospheric plasma and deduced a reaction efficiency of 10% at 300^{o}C, whilst the counter reaction ($NO_2 \rightarrow O + NO$) is active at greatly elevated temperatures. In this study evidence for this counter reaction is found in the OES spectra of the arc region, thus helping to confirm the ~1700^{o}C rotational temperature measurements in this region. In summary therefore for the APP jet discharge, the gas temperature is greatly elevated within the arc region and then rapidly cools in the afterglow region. In these two contrasting entropy regions the forward oxidation reaction (1) dominates in the flowing afterglow, while the products of the counter reaction are favored in the arc region.

Photo-diode (PD) measurements

Examples of varying the air volume and plasma cycle time (PCT) on the light intensity detected using the PD system are given in Figures 4 and 5. These measurements were obtained in the near flowing afterglow at 0-3 mm for a fixed PWM drive frequency of 25 kHz and air volume flow of 76.6 l/s. Figure 3 provides the PD measurements for a PCT of 5 and 15 % and Figure 4 is for PCT values of 40, 50 and 90 % respectively. Initial inspection of both graphs show there is temporal structure within the polychromatic emission. The temporal nature of the emission has been clarified by synchronizing the decaying edge of the pulse structures. The synchronized point is indicted by the arrow. The low PCT values (Figure 3) reveal pulse structures of 0.5 x10^{-4} s, with a decay half-life time of 0.2 x10^{-4} s and a total decay times of the order of 0.5 x10^{-4} s, beyond which there is no light emission until the next pulse. The off period for these two pulses is 0.3 x10^{-4} s, and 0.15 x10^{-4} s, which correspond to a duty cycle of (t_{on}/t_p) of approximately 5 and 15%, respectively.

For the mid values of PCT (Figure 4) a different pulse sequence structure appears. For PCT values of 40 and 50 %, two closely coupled pulses are observed with a combined on period of approximately 1 x10^{-5} s. When comparing this total on time of with their respective off period the computed effective duty cycle is to 40 and 50%. For the high value of PCT = 100 % (Figure 4) an additional pulse is presented. This pulse has approximately half the t_{on} value as compared to the pulses associated with PCT = 40 and 50 %. It is important to note here that under these conditions the power supply is delivering the maximum power it is capable to the reactor, even though there is still a portion off period.

Thermal measurements

The effect of both PCT and air flow rate on the temperature of the APP jet was investigated using infra red thermal imaging of the copper-tungsten anode-nozzle and the ceramic surface. As detailed in the experimental section the typical treatment time at a given point on the latter surface was less than 0.1 second. In addition the afterglow gas temperature at a discharge axial distance of 15 mm (Figure 2) and approximately 1 mm above the alumina ceramic surface was measured using the K-type thermocouple. This thermocouple was mounted approximately 1 mm above the ceramic surface and was plasma treated for 5 seconds. The measurement was obtained immediately after turning the plasma off. The combination of these two thermal measurement techniques allows an estimation of both the gas afterglow temperature and the heating effect of the plasma on the alumina ceramic.

Initial infra-red thermal imaging of the anode-nozzle measurements were performed at a PWM drive frequency of 21 kHz and PCT of 40% and voltage of 95%, for three different air volume flows: 35.5, 47.5 and 76.6 l/s. In all three studies a rapid rise in the anode-nozzle temperature (typically 8-10^{o}C.s^{-1}) was observed, within the first 10 seconds of turning the jet on. The nozzle temperature started to stabilize after approximately 20 seconds and the temperatures recorded at the 35.5, 47.5 and 76.6 l/s air flow rates for was 45, 50 and 60^{o}C respectively. These values subsequently converge to a stable operating nozzle temperature of approximately 55^{o}C independent of air flow rate.

Further infra red thermal imaging of the anode-nozzle and thermocouple measurements of the ceramic surface were performed at 25 kHz and a voltage of 95%. The spot temperature results of these two substrates with varying PCT are shown in Figure 5. In addition, the photo-diode RMS voltage (over a time period of 8 ms) when viewing the anode-nozzle over for this range of PCT values at 25 kHz is shown. From Figure 5 it can be seen that the anode-nozzle temperature increases with PCT percentage from 33 to 45^{o}C, the corresponding surface temperature increases from 64 to 85^{o}C. Moreover the surface temperature dataset has a distinct inflection at 15 and 75% PCT, which mirrors that observed for the PD RMS measurements.

Thermocouple measurements of the gas temperature within the flowing afterglow at 15 mm from the anode-nozzle and 1 mm above the ceramic surface were performed again under the same conditions processing conditions of 25 kHz and a voltage of 95%. The results of these measurements along with the RMS voltage of the time varying photo-diode level computed over a time period of 8 ms is given in Figures 6. In this figure the gas temperature is found to vary from 220^{o}C at 5% PCT to 284^{o}C at 100% PCT, with a mid PCT range (30% to 70%) stabilized at 238 ±1^{o}C. The shape of the temperature dataset again mirrors the computed PD RMS data.

Radial infra red mapping of the discharge interaction with the ceramic surface at 16 mm gap distance as a function of PCT percentage (10, 40 and 90%) were performed in order to provide a measure of the level of heat transfer to the surface. A typical Infra red image of the ceramic surface is shown in Figure 7. Using this thermal data it was possible to map a temperature line from the thermal data obtained for each plasma process condition as shown also in this figure. The radial distance was calibrated from the outer diameter (8 mm) of the anode-nozzle. The data presented in Figure 7 shows a symmetric temperature profile that decays outwards. Here it can be seen that the on-axis peak temperature increases with PCT percentage from 64 to 82^{o}C and the off-axis temperature has a Gaussian profile with a decay constant of one half in the range of 15-16 mm. This figure helps to provide an indication of the width of the plasma treatment obtained as the discharge passes over a surface under the processing conditions used.

Polymer surface examination

Water contact angle measurements

In this study the effect of varying the pulsed plasma cycle time on the polypropylene, polystyrene and polycarbonate water contact angle is performed. The substrates were placed a distance of 16 mm from the anode-nozzle. The jet was then moved at 500 mm.sec^{-1} across the samples in a raster pattern with a line spacing of 4 mm. The plasma processing parameters, (PWM drive frequency = 25 kHz, 95% voltage, and 76.6 l/s air volume flow), were chosen following an iterative study of the plasma activation of PET film. In this experiment the Plasma cycle time, PCT, was varied from 10 to 100% in 10% intervals. An additional point at 5% PCT was examined in order to observe the effect of low PCT. From the information detailed in Figure 7, these treatment parameters lead to an effective ceramic temperature range of 55 to 82 degrees, within each scan (with a 5 second treatment). The contact angle was measured one hour, one day and five days after activation in order to explore the hydrophobic recovery of the polymers.

For the untreated polystyrene and polycarbonate surfaces the WCA were close to 93^{o} and 83^{o} respectively. The APP jet treatment typically reduces the surface WCA (typically 20-30 degrees), when measured in the first hours after treatment. For the polystyrene and polycarbonate surfaces, the water contact angle remained almost constant at all treatments between 5% and 70% PCT (Figure 8 and 9). The WCA value then decreased to lower values with the more intense plasma obtained above 80% PCT values. In the case of polypropylene the behaviour is different. The WCA of the untreated polymer is close to 90^{o}, APP jet treatment induces a small WCA reduction (10^{o}) in the mid PCT range (30 to 70%) followed by an increase in WCA at higher PCT values (Figure 10). This rise in water contact angle may be as a result of thermal damage caused to the polymer surfaces during the plasma treatment process. As this effect is not observed for the polycarbonate or polystyrene samples, the increase in contact angle for polypropylene at higher PCT levels may be associated with its significantly lower glass transition temperature. This polymer would thus be more susceptible to thermal damage arising from the plasma treatment. From the thermal studies the 160^{o}C melting temperature of polypropylene is not attained with the APP jet however the increase in contact angle at higher PCT levels would indicate some deterioration in the surface of the polymer.

Polypropylene AFM and XPS examination

To investigate how the PCT level influenced the polypropylene surface morphology, its surface roughness (Ra and Rq) before and after plasma treatment was measured using AFM. These measurements were obtained at five different points on the polymer surfaces. Starting from an initial value of 4.8 and 5.76 nm, respectively, the Ra and Rq values increased to 5.1 and 6.4 nm respectively at a PCT value of 30%. With treatment at a PCT value of 100% there was no significant change in roughness with the Ra and Rq values of 4.9 and 6.5 nm respectively. These values are depicted as upside-down triangles in Figure 10. These surface roughness values appear to be independent of PCT (%) in contrast to the WCA measurements. Similar results were reported previously by P. Pedrosa *et al* [21] for roughness changes following the plasma treatment of polypropylene using argon and argon + oxygen plasmas at atmospheric pressure. In this study it was concluded that variations in Ra may not significantly correlate with the WCA (hydrophilicity) after plasma treatment. In order to obtain an understanding of how the surface chemistry of the polymer was altered with plasma treatment an XPS examination was carried out for the untreated polypropylene and the polymer after exposure to 30 and 100% PCT. The results of this study are given in Table 1. In addition to carbon (C) and oxygen (O) other

elements detected in the untreated polymer were calcium and nitrogen at concentrations of 1.1 and 0.9% respectively. From table 1 it is clear that with increased plasma exposure there is a significant increase in the level of oxidation of the polymer. The higher levels of oxidation obtained after the 100% PCT treatment may be associated with the thermal decomposition of the surface layer.

Conclusions

This study investigated the influence of processing conditions of plasma cycle time (PCT), air flow rate and gap distance on the formation of active species in the air plasma, in addition to the heating effect of the plasma and the level of polymer activation.

The air APP jet discharge was found to have two distinct plasma regions: the blown arc and flowing afterglow region. Photo-diode measurements reveal the arc region has a time modulated polychromic light emission that follows the PCT (effective duty cycle) of applied power from the power supply. Optical emission spectroscopy measurements reveal air is highly dissociated (NOγ bands (λ = 236-258 nm), the second positive system of molecular N_2 ($C^3\Pi^+u$-$B^3\Pi^+_g$) and at λ = 391 nm the $v = 0 \rightarrow 0$ band of the first positive nitrogen ions N_2^+ ($B^2\Sigma^+u$-$X^2\Sigma^+_g$), atomic H-Balmar-α line at λ = 656 nm, nitrogen and the O ($3p^5P$–$3s^5S$) at λ = 777 nm). Simulation of the second positive system of molecular nitrogen at λ = 380 nm produced a rotational temperature in the range of 1709 ±100^{o}C at 25 kHz to 1761 ±100^{o}C at 19 kHz. Using a thermocouple measurement the flowing afterglow at an axial-line distance of 15 mm the gas temperature was found to be considerably cooler at a few hundred ^{o}C. This significantly influenced the types of active species observed (NO_2* continuum is formed with the second positive system of molecular N_2).

Infra-red thermal imaging and thermocouple measurements were used to measure the temperature both at and close to (thermocouple) the treated surfaces. From this study it was demonstrated that there was a strong correlation between the substrate temperatures and the percentage PCT applied. This however was not a linear relationship, step increases being observed up to 20% PCT and above 80% PCT levels. The more intense plasma obtained at the higher PCT levels gave higher surface temperatures and higher levels of polymer activation. In the case of polypropylene there was evidence for some polymer decomposition based on changes in the contact angle value and also higher levels of oxidation observed by XPS examination. This polymer had the lowest T_g of the three polymers investigated.

Acknowledgements

This work is supported by Science Foundation Ireland Grant 08/SRC11411. The authors acknowledge K. Niemi for the simulation and measurement of the rotation temperature of the N_2 $v = 0 \rightarrow 2$ rotational band ($C^3\Pi^+_u$ –$B^3\Pi^+_g$) at λ = 380 nm.

References

[1] M. J. Shenton, M. C. Lovell-Hoare and G. C. Stevens, Adhesion enhancement of polymer surfaces by atmospheric plasma treatment, J. Phys D: Appl. Phys, Vol.34, (2001), 2754-2760

[2] A. Kruse, G. Kruger, A. Baalmann and O. D. Hennemann, Surface pretreatment of plastics for adhesive bonding, J. Adh. Sci. and Tech, Vol.9, (1995), 1611-1621.

[3] M. Strobel, N. Sullivan, M. Branch, J. Park, M. Ulsh, R. Kapaun and B. Leys, Surface modification of polypropylene film using N_2O-containing flames, J. Adh. Sci. and Tech, Vol.10, (2000), 1243-1264

[4] D. Briggs, D.G. Rance, C.R. Kendall and A.R. Blathe, Surface modification of poly(ethylene terephthalate) by electrical discharge treatment, J. polymer, Vol.21, (1980), 895-900.

[5] S. L. Kaplan Plasma processes in the plastics industry, *35th Ann. Tech Conf. Soc. Of Vacuum Coaters*, (1992), 273-277.

[6] M. Noeske, J. Degenhardt, S. Strudthoff, U. Lommatzsch, Plasma treatment of five polymers at atmospheric pressure: surface modifications and the relevance for adhesion, Int. J. of Adhesion and adhesives, Vol.24, (2004), 171-177.

[7] D. P. Dowling, B. Twomey and G. Byrne, Deposition of functional coatings using an-inline atmospheric pressure plasma apparatus, *48th ann. Conf. society of vacuum coaters*, (2005), 214-218.

[8] L. J. Gerenser, Surface chemistry of plasma treated polymers, *Handbook of thin film process technology*, ed D.B. Glocker, S. L. Shah. Ch.E3.1, (1996)

[9] F. Arefi-Khonsari M. Tatoulian, F. Bretagnol, O. Bouloussa, F. Rondelez., Processing of plasma technologies, *Surface and coating technologies*, Vol.200, (2005), 14-20.

[10] A. Ramamoorthy, J. Mohan, N. Murphy, A. Ivankovic and D. P. Dowling, Enhanced Carbon/Epoxy composite fracture toughness achieved using atmospheric pressure plasma treatments, , *Proceedings of the 33rd annual Adhesion Society Meeting*, Feb 2010, Daytona Beach, Florida.

[11] M. E. R. Shanahan and C. Bourges-Monnier, Effects of plasma treatment on the adhesion of an epoxy composite, Int. J. of adhesion and adhesives, Vol.16, No.2, (1996) 129-135.

[12] S. A. Pirzada, A. Yializis, W. Decker, and R. E. Ellwanger, Plasma treatment of polymer films, *42nd ann. Conf. society of vacuum coaters*, (1999), 301-306.

[13] U. Lommatzsch, D. Pasedag, A. Baalmann, G. Ellinghorst and Hans-Erich Wagner, Atmospheric pressure plasma jet

treatment of polyethylene Surfaces for adhesion improvement, Plasma Process. Polym. 2007, 4, S1041–S1045.
[14] A. Baltazar-y-Jimenez, M. Bistritz, E. Schulz, A. Bismarck. Atmospheric air pressure plasma treatment of lignocellulosic fibres: Impact on mechanical properties and adhesion to cellulose acetate butyrate. Composites Science and Technology, (2008), 68, 215–227,
[15] P. Scopece, A. Viaro, R. Sulcis, I. Kulyk, A. Patelli and M. Guglielmi, SiOx based gas barrier coatings for polymer substrates by atmospheric pressure plasma jet deposition, Plasma Process. Polym. (2009), Vol.6, S705-S710.
[16] U. Lommatzsch and J. Ihde, Plasma polymerization of HMDSO with an atmospheric pressure plasma jet for corrosion protection of aluminum and low-adhesion surfaces. Plasma Process. Polym. (2009), Vol.6, 642–648.
[17] P. Bringmann, O. Rohr, F. J. Gammel, I. Jansen, Atmospheric pressure plasma deposition of adhesion promotion layers on aluminum. Plasma Process. Polym. (2009), Vol.6, S496-S502.
[18] I. S. Grigoriev, and E. Z. Meilikhov, Handbook of Physical Quantities, CRC Press, Boca Raton, (1997). ISBN 10 0849328616
[19] C. J. Renger, S. J. Burrows and R. A. Shanks. Processing, crystallization and dynamic mechanical analysis of high molar mass polysiloxane-modified PP/$CaCO_3$ Composites. J. Appl. Polym. Sci. (2001), 82, 3091-3098.
[20] C. Canal, F. Gaboriau, A. Vílchez, P. Erra, M. Garcia-Celma, and J. Esquena. Topographical and wettability effects of post-discharge plasma treatments on macroporous polystyrene-divinylbenzene solid foams. Plasma Process. Polym. (2009), Vol.9, 686-692.
[21] P. Pedrosa, J-M. Chappé, C. Fonseca, A. V. Machado, J. M. Nóbrega, and F. Vaz. Plasma surface modification of polycarbonate and poly(propylene) substrates for biomedical electrodes. Plasma Process. Polym. (2010), Vol.7, 676-686.
[22] P. Fauchais, A. Vardelle. Thermal Plasmas. IEEE Trans Plasma Sci, (1997), Vol.25, 1258-1280.
[23] V. Rat, J-F. Coudert, A. Denoirjean and G. Montavon, Blown arc plasma source for the elaboration of finely structured coatings. The Open Plasma Physics Journal, 2009, 2, 133-149.
[24] S. Castagno, R. D. Curry, and E. Loree, Analysis and comparison of a fast turn-on series IGBT stack and high voltage rated commercial IGBTs. IEEE Trans, Plasma Sci. (2006), Vol.34, 1692-1696,
[25] V. J. Law, M. Tewordt, D. C. Clary and G. A. C. Jones. 300 kHz pulse plasma etching of GaAs using a mixture of $ClCH_3$ and H_2. J Vac, Sci, Technol. (1993), B11(6), 2262-2265.
[26] D. Paul, V. J. Law and G. A. C. Jones. $Si_{1-x}Ge$ pulse-plasma etching using CHF_3 and H_2^*. J. Vac. Sci. Technol. (1995) **B13**(6), 2234-2237.
[27] H. Hillborg, and U. W. Gedde, Hydrophobicity recovery of polydimethylsiloxane after exposure to corona discharge, Polymer, (1998), Vol.39, 1991-1998
[28] P. A. F Herbert, L. O'Neill, J. Jaroszynska-Wolinska. Soft plasma polymerization of gas state precursors from an atmospheric pressure corona plasma discharge, J. Chem, Mater. (2009), 21, 4401-4407.
[29] C. E. Nwankire, V. J. Law, A. Nindrayog, B. Twomey, K. Niemi, V. Milosavljević, W. G. Graham, and D. P. Dowling. Electrical, thermal and optical diagnostics of an atmospheric plasma jet system. Plasma Chem, Plasma Processing, (2010) 30, 537–552
[30] W. B. Pearse, and A. C. Greydon. Identification of molecular spectra. Chapman & Hall London, 2001.
[31] B. Twomey, A. Nindrayog, K. Niemi, W. G. Graham, D. P. Dowling, Correlation between the electrical and optical properties of an atmospheric pressure plasma during siloxane coating deposition, Plasma Chem Plasma Process. (2010). PCPP-10-SV-0006.
[32] M. Sutoh, Y. Morioka, and M. Nakamura. Absolute rate constant for the chemiluminescent reaction of atomic oxygen with nitric oxide. J. Chem. Phys. (1980), Vol.72, 20-24.
[33] B. M. Penetrante, R. M. Brusasco, B. T. Merritt and G. E. Vogtlin. Environmental applications of low-temperature plasmas. Pure Appl. Chem, (1999).Vol.71, 1829-1835.
[34] L. Bárdoš. Afterglow and decaying plasma CVD systems. Vacuum. (1988), Vol.38, 637-642.

Figure Captions

Figure 1: Photograph (left) and schematic (right) of the anode-nozzle, arc and flowing afterglow. Conditions: PWM driving frequency = 19 kHz, PCT = 20 (%), 95% output voltage and air volume flow = 37.5 l/s.

Figure 2: Low resolution OES (200-850 nm) of discharge afterglow as a function axial distance (0, 5, 10, and 15 mm). PWM drive frequency 25 kHz, PCT = 100 (%), and air volume flow = 76.6 l/s.

Figure 3: Temporal variation of PD Voltage of near-field flowing afterglow for 5% and 15 (%) PCT at a PWM drive frequency = 25 kHz. Process conditions: nozzle-to-surface gap distance = 16 mm, air volume flow rate = 76.6 l/s.

Figure 4: Temporal variation of PD Voltage of near-field flowing afterglow for PCT = 40 (%), 50 (%) and 90 (%), at 25 kHz. Process conditions: nozzle-to-surface gap distance = 16 mm, air volume flow = 76.6 l/s.

Figure 5: Infra red thermal imaging measurement of the anode-nozzle and ceramic surface for a 5 second exposure as a function of PCT (%). Power conditions: 25 kHz, air volume flow = 76.6 l/s and gap distance 16 mm. Also given is the computed photo-diode time varying voltage level as viewed at the anode-nozzle for the same power conditions.

Figure 6 Thermocouple measurements ~ 1 mm above of ceramic surface for a 5 second exposure as a function of PCT (%). Power conditions: 25 kHz, air volume flow = 76.6 l/s and gap distance 16 mm. Also given is the computed photo-diode time varying voltage level as viewed at the anode-nozzle for the same power conditions.

Figure 7: Infra-red thermal image of air discharge at a gap distance of 16 mm from surface. PCT (%). Power conditions: PWM 25 kHz, air volume = 76.6 l/s (left). Infra-red estimation of ceramic surface temperature for PCT values of 10, 40 and 90% (right).

Figure 8: Polystyrene water contact angle (recovery time; 1hr, 1day and 5days) vs. PCT (%). Power conditions: PWM 25 kHz, air volume = 76.6 l/s and gap distance 16 mm.

Figure 9: Polycarbonate water contact angle (recovery time; 1hr, 1day and 5days) vs. PCT (%). Power conditions: PWM 25 kHz, air volume = 76.6 l/s and gap distance 16 mm.

Figure 10: Polypropylene water contact angle (recovery; time 1hr, 1day, 5days) vs. PCT (%). Power conditions: PWM 25 kHz, air volume = 76.6 l/s and gap distance 16 mm.

Figure 1

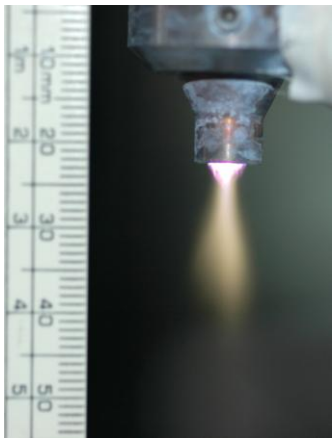

Photograph of Anode-nozzle
with arc and afterglow

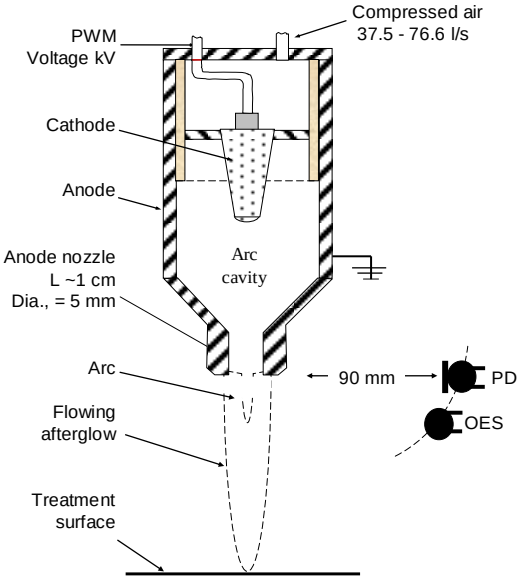

Figure 2

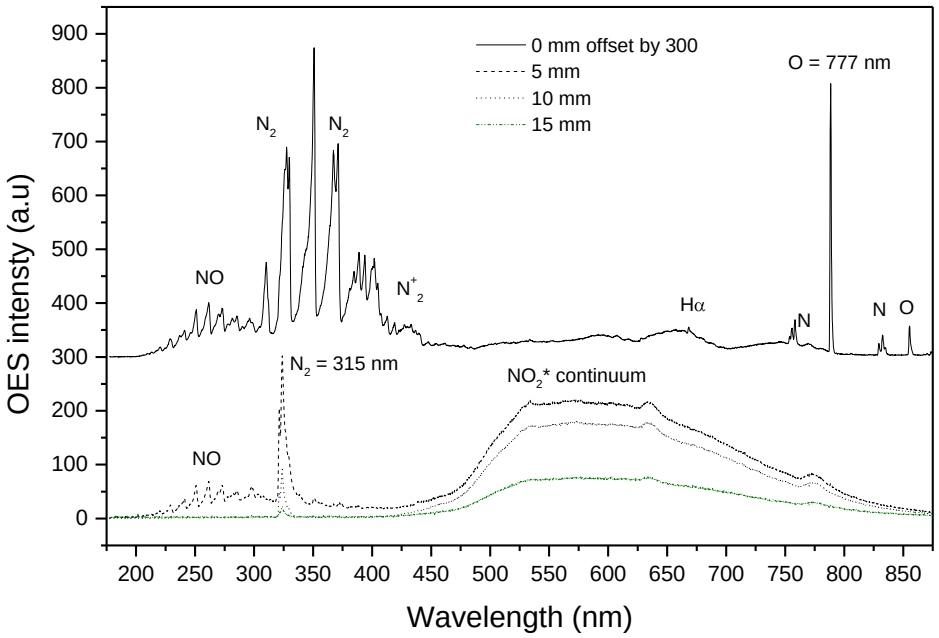
0 mm offset by 300
5 mm
10 mm
15 mm
O = 777 nm
N2
N2
NO
N+2
Hα
N
N
O
N2 = 315 nm
NO2* continuum
NO
OES intensty (a.u)
Wavelength (nm)
0
100
200
300
400
500
600
700
800
900
200
250
300
350
400
450
500
550
600
650
700
750
800
850

Figure 3

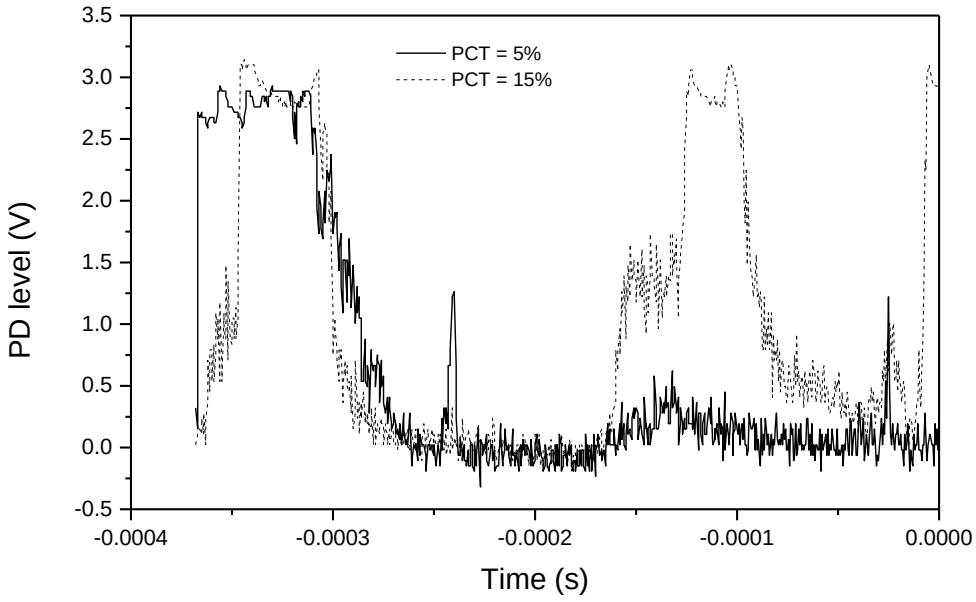
PCT = 5%
PCT = 15%
PD level (V)
Time (s)
3.5
3.0
2.5
2.0
1.5
1.0
0.5
0.0
-0.5
-0.0004
-0.0003
-0.0002
-0.0001
0.0000

Figure 4

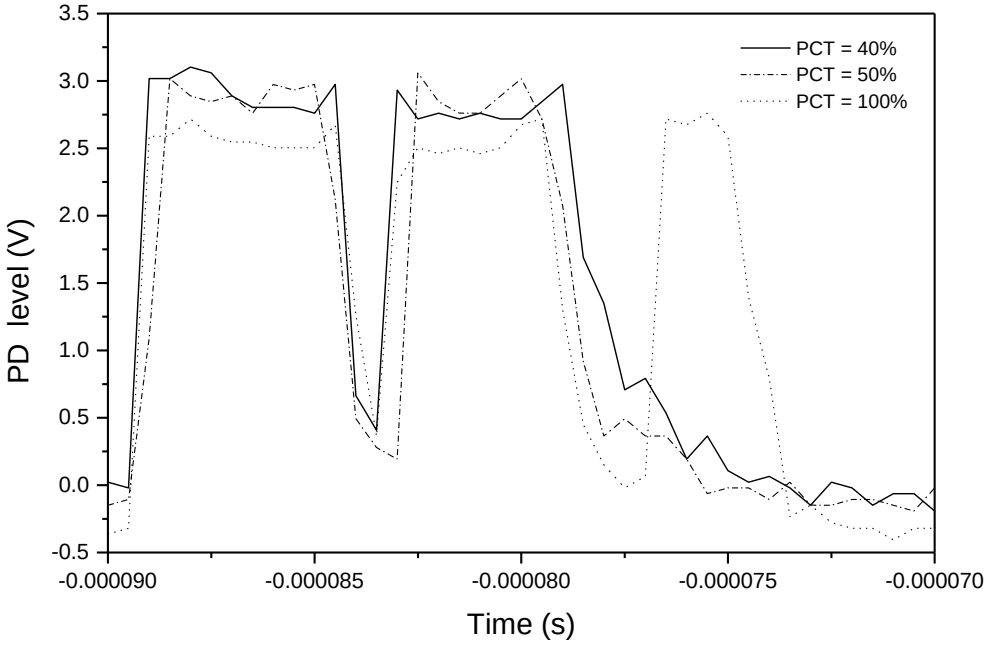
PCT = 40%
PCT = 50%
PCT = 100%
PD level (V)
Time (s)
3.5
3.0
2.5
2.0
1.5
1.0
0.5
0.0
-0.5
-0.000090
-0.000085
-0.000080
-0.000075
-0.000070

Figure 5

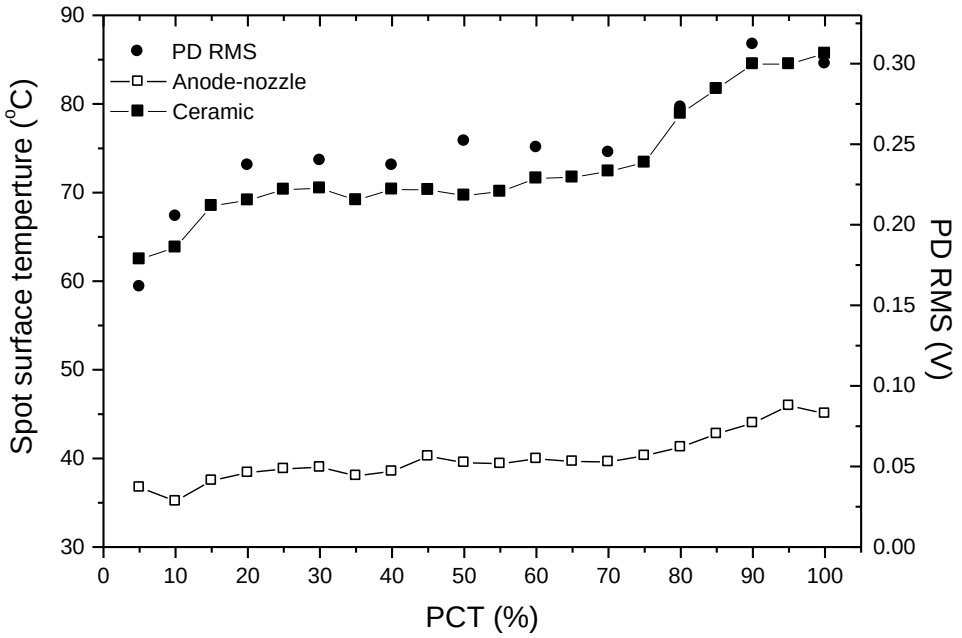
PD RMS
Anode-nozzle
Ceramic
Spot surface temperture (°C)
PD RMS (V)
PCT (%)
90
80
70
60
50
40
30
0.30
0.25
0.20
0.15
0.10
0.05
0.00
0
10
20
30
40
50
60
70
80
90
100

Figure 6

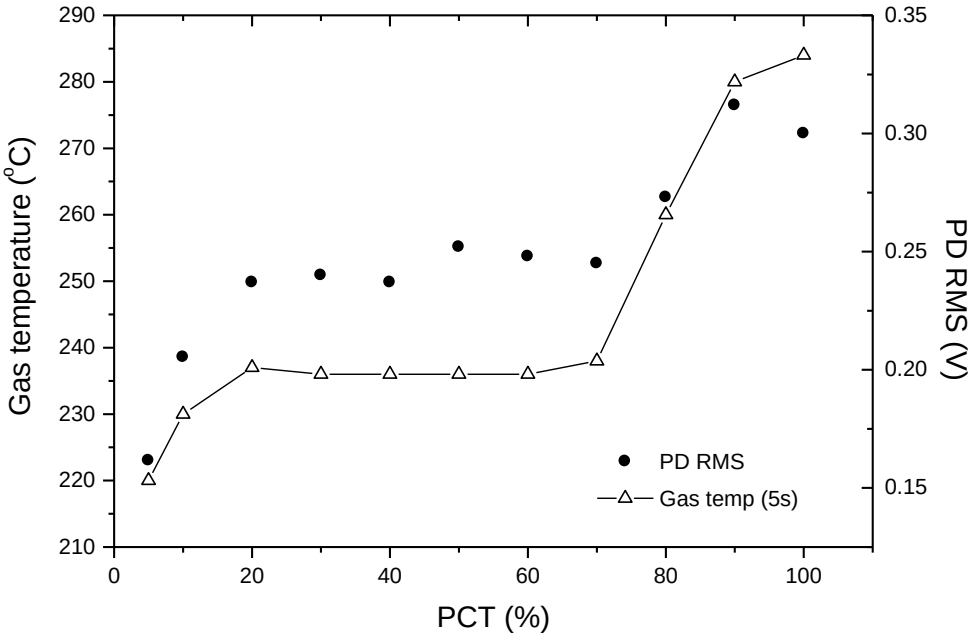
Gas temperature (°C)
PD RMS (V)
PCT (%)
PD RMS
Gas temp (5s)
290
280
270
260
250
240
230
220
210
0.35
0.30
0.25
0.20
0.15
0
20
40
60
80
100

Figure 7

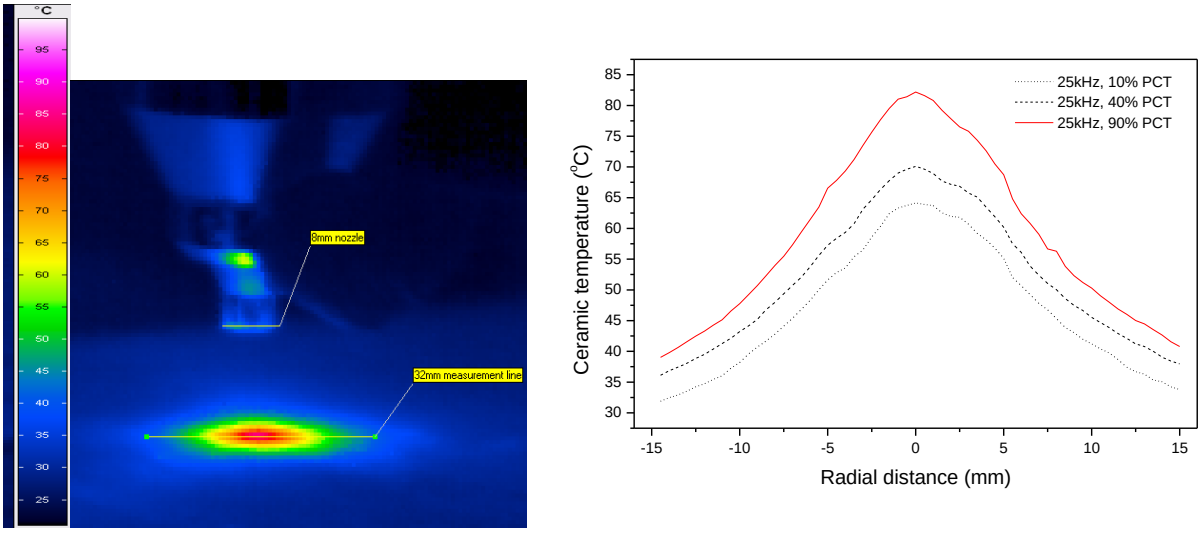
°C
95
90
85
80
75
70
65
60
55
50
45
40
35
30
25
8mm nozzle
32mm measurement line
25kHz, 10% PCT
25kHz, 40% PCT
25kHz, 90% PCT
Ceramic temperature (°C)
Radial distance (mm)
85
80
75
70
65
60
55
50
45
40
35
30
-15
-10
-5
0
5
10
15

Figure 8

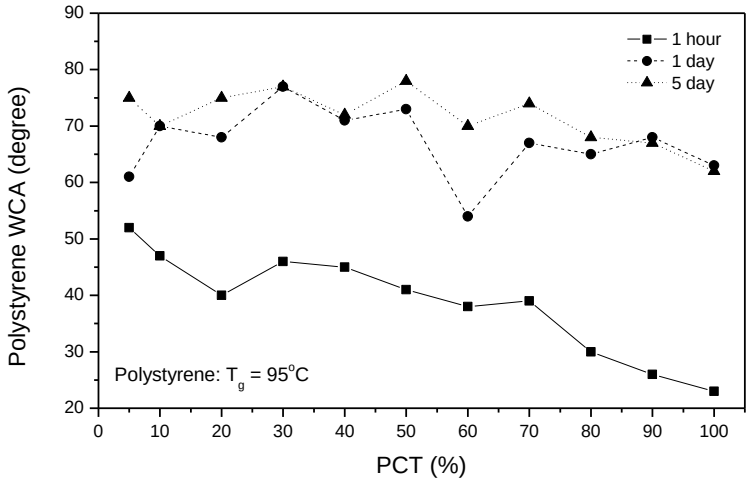
Polystyrene WCA (degree)
PCT (%)
1 hour
1 day
5 day
Polystyrene: T_g = 95°C
90
80
70
60
50
40
30
20
0
10
20
30
40
50
60
70
80
90
100

Figure 9

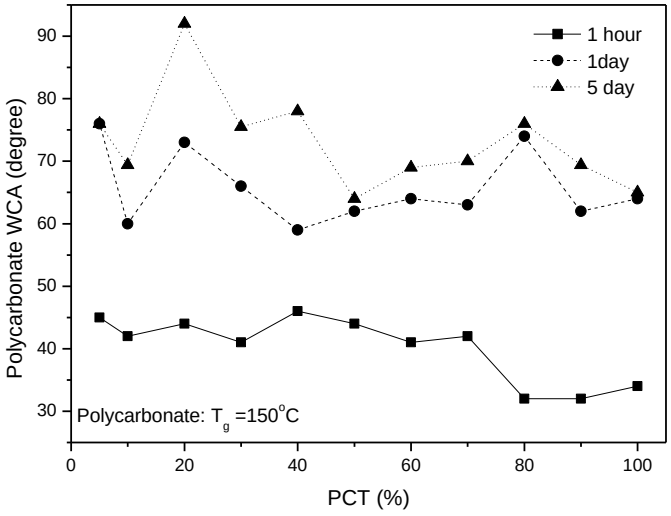
1 hour
1day
5 day
Polycarbonate WCA (degree)
PCT (%)
Polycarbonate: T_g =150°C
90
80
70
60
50
40
30
0
20
40
60
80
100

Figure 10

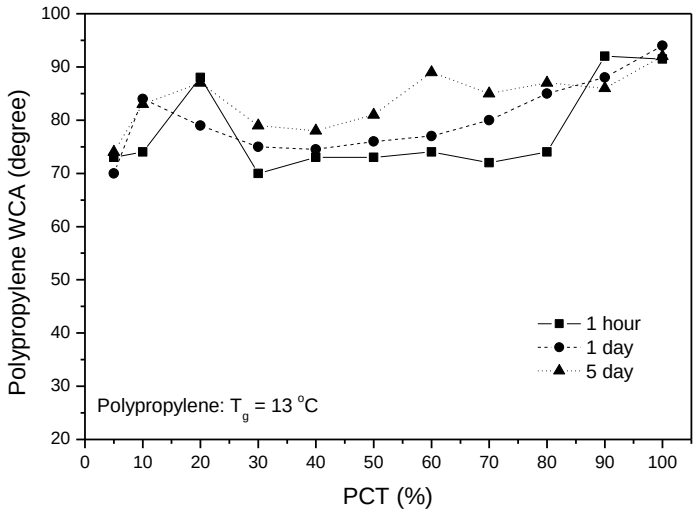
Polypropylene WCA (degree)
PCT (%)
1 hour
1 day
5 day
Polypropylene: T_g = 13 °C

Table 1: XPS analysis of the Polypropylene substrate both prior to treatment and also post treatment for two different PCT settings, 30 % and 100%.

Treatment	C%	O%
Untreated PP	90.7	7.5
Treated 30% PCT	87.1	12.9
Treated 100% PCT	85.5	14.5